Saudi Pharmaceutical Journal 32 (2024) 102208

HOSTED BY

Contents lists available at ScienceDirect

Saudi Pharmaceutical Journal

journal homepage: www.sciencedirect.com

Original article

Bioadhesive hybrid system of niosomes and pH sensitive *in situ* gel for itraconazole ocular delivery: Dual approach for efficient treatment of fungal infections

Mohamed M. Badran [a,*], Areej Alsubaie [a], Mounir M. Salem Bekhit [a], Abdullah H. Alomrani [a], Aliyah Almomen [b], Mohamed Abbas Ibrahim [a], Doaa Hasan Alshora [a]

[a] Department of Pharmaceutics, College of Pharmacy, King Saud University, Riyadh 11451, Saudi Arabia
[b] Department of Pharmaceutical Chemistry, College of Pharmacy, King Saud University, Riyadh 11495, Saudi Arabia

ARTICLE INFO

Keywords:
Itraconazole
Niosomes
Bioadhesive
In situ gel
Ocular delivery
Antifungal activity

ABSTRACT

Itraconazole (ITZ) is a highly effective antifungal agent. However, its oral application is associated with systemic toxicity and poor topical use. The present study aims to improve the antifungal activity of ITZ by loading it into bioadhesive niosomes. This approach is considered to enhance the ocular permeation of ITZ, thereby boosting its efficacy against fungal infections. Therefore, it was encapsulated into niosomes (F1) and subsequently coated with hyaluronic acid (HA; F2), chitosan (CS; F3), or a bilayer of CS/HA (F4). In addition, they were further incorporated into pH-sensitive *in situ* gels. This dual approach is expected to increase the amount of corneal-permeated ITZ, facilitating more effective management of ocular fungal infection.

Firstly, the niosomes were prepared by hydrating proniosomes using span 60, cholesterol, and phospholipid. ITZ-niosomes showed an increase in vesicle size from 165.5 ± 3.4 (F1) to 378.2 ± 7.2 nm (F3). The zeta potential varied within −20.9 ± 2.1 (F1), −29.5 ± 3.1 (F2), 32.3 ± 1.9 (F3), and 22.6 ± 1.3 mV (F4). The high EE% values ranged from 78.1 ± 2.2 % to 86.6 ± 2.9 %. Regarding ITZ release, F1 demonstrated a high release profile, whereas bioadhesive niosomes showed sustained release patterns. Furthermore, *in situ* gels containing niosomes displayed excellent gelling capacity and viscosity. Remarkably, F3 laden-*in situ* gels (F3-ISG) demonstrated the highest *ex vivo* corneal permeability of ITZ and antifungal activity with a safety effect. These results indicate that F3-ISG presents a promising strategy for boosting the ocular delivery of ITZ, that could help in treating ocular fungal infections.

1. Introduction

Fungal infection is one of the common diseases that affect the eye (Kumar et al., 2022). For instance, fungal keratitis causes an inflammation of the cornea due to fungal infection, which may cause corneal epithelial damage and stromal inflammation (Bongomin et al., 2017), which could lead to corneal scarring and visual impairment. Various factors may increase fungal eye infections, such as the use of immunosuppressive drugs, broad-spectrum antibiotics, and contact lenses (Mehrandish & Mirzaeei, 2020). Therefore, it is important to deliver the drug to the cornea, the main location of infections, effectively (Bhattacharjee et al., 2019). Developing effective drug delivery for eye infections encounters significant challenges due to the physiological and anatomical characteristics of the eye (Kumar et al., 2022). Conventional ophthalmic preparations face difficulties in delivering and maintaining a sufficient amount of the drug within the cornea region for a long time. Itraconazole (ITZ) is a commonly used antifungal agent for eradicating many fungal infections (Permana et al., 2021). ITZ has very low water solubility (<1 μg/ml), high lipophilicity (log *p:* 5.66 at a pH of 8.1), and relatively large molecular weight (705.64 Da) (Alomrani et al., 2015). These properties lead to limited corneal permeation, resulting in reduced ocular bioavailability. Therefore, nanocarriers have emerged as a promising solution for addressing these challenges. They offer several benefits for ocular drug delivery, including enhancing stability, extended drug release, improving bioavailability, and targeting delivery (Bhattacharjee et al., 2019). The ocular nanocarriers can also overcome the limitations of regular eye drops by remaining longer, penetrating better, and reaching the infection site in a sufficient amount of the drugs.

* Corresponding author at: Department of Pharmaceutics, College of Pharmacy, King Saud University, P.O. Box 2457, Riyadh 11541, Saudi Arabia.
E-mail address: mbadran@ksu.edu.sa (M.M. Badran).

https://doi.org/10.1016/j.jsps.2024.102208
Received 26 August 2024; Accepted 21 November 2024
Available online 22 November 2024

Ocular nanocarriers can also be designed to target the infected site, localize, and prolong the release of the antifungal drug. This approach could improve the effectiveness of treatment by reducing the requirement of frequent dosing. Niosomes are vesicular drug delivery systems, which usually made of non-ionic surfactants and cholesterol. Niosomes hold great potential as drug carriers due to their biocompatibility, biodegradability, and non-immunogenic properties (Bhattacharjee et al., 2019). Niosomes offer significant advantages over liposomes, mainly in terms of stability and cost-effectiveness of manufacturing. Niosomes in ophthalmic drug delivery demonstrated potential effectiveness in treating eye conditions such as glaucoma and microbial infections and protecting the drug from tear enzymes (Ge et al., 2019; Gharbavi et al., 2018). The niosomes were fabricated by the rehydration of proniosomes (Ajrin & Anjum (2022). The proniosomes have attracted great attention in various drug delivery (Alshora et al., 2023; Darson et al., 2023). Abu El Enin et al. (2019) (Abu El-Enin et al., 2019) prepared a proniosomal gel by coacervation phase separation with a high EE% and sustained fluconazole release. The proniosomes were fabricated to improve the ocular bioavailability of lomefloxacin HCl with good therapeutic outcomes (Ajrin & Anjum, 2022). Furthermore, proniosomes containing brimonidine tartrate were also successfully developed for glaucoma management without eye irritation (Emad Eldeeb et al., 2019). Additionally, tacrolimus-loaded niosomes for treating corneal graft rejection have exhibited great promise for future clinical applications (Zeng et al., 2016).

In addition, the niosomes could be coated by bioadhesive agents to provide mucoadhesive properties and prolong the adhering of the nanocarriers to the ocular surface for a long time. Increasing resident time usually leads to high corneal drug absorption and bioavailability, and improves patient compliance. Chitosan (CS) has excellent mucoadhesive properties that facilitate the interaction with mucous membranes, promoting topical drug penetration (Idrees et al., 2020; (Pandit et al., 2021; Supachawaroj et al., 2021). CS-coated niosomes succeeded to extend the ocular retention time and facilitate the transcorneal permeation of gatifloxacin (Zubairu et al., 2015). Moreover, hyaluronic acid (HA) have a significant mucoadhesion characterization that effectively prolonged the contact time of many drugs and improving their ocular bioavailability (Landucci et al., 2023; Zhang et al., 2021). Moreover, the CS and HA-bilayer coated niosomes could provide synergistic effects for various biomedical applications, particularly in enhancing the mucoadhesive properties (Sionkowska et al., 2020). Therefore, this work is designed to optimize ITZ-loaded niosomes by modifying their composition using span 60, phospholipids (lipoid S100), and cholesterol. Furthermore, the impact of HA and CS as single or combined double layers on the ITZ-loaded niosomes was also investigated. For efficient ocular ITZ delivery, the optimized formulae were incorporated into *in situ* gelling polymers and subjected to antifungal activity study, *in vitro*, and *in vivo* characterization. This hybrid system may offer promising results in enhancing the ocular availability of ITZ (Padmasri & Nagaraju, 2021).

2. Materials and methods

Itraconazole (ITZ) was purchased from Betapharma (Shanghai, China). Lipoid S100 (Soybean phosphatidylcholine content >94 %) was obtained from Lipoid GmBH (Ludwigshafen, Germany). Cholesterol and low molecular weight chitosan (50~190 kDa; 91.5 % deacetylated) was obtained from Sigma-Aldrich Co., LLC (St. Louis, MO, USA). Span 60 was obtained from Koch-light Laboratories Ltd., (Colnbrook Buck, England). Hyaluronic acid sodium salt (Molecular weight; 1000–1800 kDa) was obtained from Bloomage Freda Biopharm Co., Ltd. (Jinan, China). Acetonitrile, methanol, and ethanol HPLC grade be obtained from Fisher Scientific, (Leicestershire, UK).

2.1. Preparation of ITZ loaded-bioadhesive niosomes

The proniosomes, which serve as the primary step for niosomal preparation, were prepared by a coacervation-phase separation approach (El-Emam et al., 2023). Briefly, span 60 (90 mg), lipoid S100 (90 mg), and cholesterol (10 mg) were dispersed in ethanol (5 mL) and heated at 65 °C with continuous stirring (500 rpm) to ensure complete dissolution of all components. Then, 10 mg of ITZ was added to this solution and heated at 65 °C for 10 min with vortexing for 10 min to get a homogenous mixture. Preheated distilled water (0.2 mL) was added at 65 °C under vortexing for 3 min. Afterward, proniosomal gels were obtained after cooling at room temperature. Details of the formualtions are illustrated in Table 1.

To produce ITZ-loaded conventional niosomes (F1), ITZ-proniosomal gel was reconstituted with 10 mL of PBS (pH 7.4) under continuous stirring for 2 h at room temperature. For the preparation of HA-bioadhesive ITZ niosomes (F2), 10 mL of PBS (pH 7.4, which contains 0.2 % HA, w/v) was added to ITZ-proniosomal gel under stirring at 25 °C (Nemr et al., 2022; Zeng et al., 2016). While CS-bioadhesive ITZ niosomes (F3) were prepared by adding 10 mL of a 0.5 % w/v CS solution (dissolved in 0.1 % v/v acetic acid) to ITZ-proniosomal gel under stirring at 25 °C (Tulbah et al., 2023). Furthermore, bi-layered niosomes were achieved by successive additions of CS and HA solutions onto ITZ-proniosomal gel according to electrostatic interaction as described in a previous method with minor modification (Jeon et al., 2015). Firstly, 5 mL of HA solution was added dropwise into ITZ-proniosomes as previously described, followed by adding 5 mL of CS solution dropwise using the previous procedure. The positively charged CS layer is physically attached to the negatively charged HA-bioadhesive niosomes, leading to double-layered niosomes (F4). All hydrated mixtures were then left overnight at 4 °C for swelling, followed by bath sonication for 1 h and probe sonication for 10 min under ice. The resulting formulations were then light centrifuged at 6000 rpm for 5 min to remove any titanium particles (out of the probe sonicator) and large particles. The bioadhesive niosomes were centrifuged at 30 rpm for 1 h at 4 °C to remove excess CS/HA and washed twice with distilled water. Moreover, the obtained formulations were prepared under aseptic conditions, as PBS was filtered through a 0.22-μm membrane filter, glassware was autoclaved, and the procedure was done in a laminar flow hood. The conventional and bioadhesive niosomes were stored at 4 °C for further studies.

2.2. Characterization of ITZ loaded-bioadhesive niosomes

2.2.1. Vesicle size and zeta potential measurements

The mean vesicle size, PDI, and zeta potential of the freshly prepared niosomes were determined using a Zetasizer Nano ZS (Malvern Instruments, Worcestershire, UK) at 25 °C and 90°. Each niosomal dispersion (10 μL) was diluted to 1 mL with deionized water before measurement. The measurements were run three times.

2.2.2. Determination of the entrapment efficiency

The entrapment efficiency (EE%) values of the obtained niosomes were determined by the indirect method using the ultracentrifugation

Table 1
Composition of ITZ-loaded bioadhesive niosomes.

Ingredients/Codes	F1	F2	F3	F4
Span 60 (mg)	90	90	90	90
Lipoid S100 (mg)	90	90	90	90
Cholesterol (mg)	10	10	10	10
ITZ (mg)	10	10	10	10
Ethanol (μL)	50	50	50	50
PBS (mL)	10	–	–	–
HA (0.2 %) mL	–	10	–	5
CS (0.5 %) mL	–	–	10	5

technique (Alomrani et al., 2015). The niosomal dispersions were ultracentrifuged at 40000 rpm at 4 °C for 30 min. The amount of ITZ in the supernatant and the total preparation were determined after proper dilution with acetonitrile. Then, the content of ITZ was analyzed using the HPLC. Then, the EE% was calculated according to the following equation:

$$EE\% = \frac{ITZ(t) - ITZ(f)}{ITZ(t)} \times 100$$

ITZ (t) is the total drug amount and ITZ (f) is the free drug amount in the supernatant after centrifugation at 40000 rpm.

The ITZ was determined by a modified reversed-phase HPLC method (Alhowyan et al., 2019) using PerkinElmer™ HPLC system. ITZ sample (30 µL) was analyzed using a mobile phase formed of a mixture of deionized water and acetonitrile in a ratio of 30:70 (v/v) adjusted at pH 3.5 using glacial acetic acid. The mobile was passed through a reversed-phase C_{18} column (PerkinElmer, 4.6 × 150 mm, 5 µm particle size) at a flow rate of 1.2 mL/min and room temperature. The detection of ITZ was performed using a UV detector set at a wavelength of 245 nm. The HPLC system was monitored by "TotalChrom Workstation" software, version 6.3.1 (2006).

2.2.3. Transmission electron microscopy (TEM)

The morphology of the obtained niosomes was observed by TEM (JEM-2000EX II, JEOL, Tokyo, Japan). A drop of the niosome was suitably diluted and negatively stained with a 1 % phosphotungstic acid solution. The stained niosome was then subjected to TEM microscopical investigation.

2.2.4. Stability study

The purpose of the stability study was to inspect the changes in the physicochemical properties of the obtained niosomal dispersions over time. The niosomes were kept in closed vials for 2 months in a stability chamber at 4 °C and 25 °C, with 60 % relative humidity. The samples were taken to measure the particle size and zeta potential (Allam et al., 2019). The stability test was performed in triplicate.

2.3. Preparation of ITZ-bioadhesive niosomes laden-in situ gels

The obtained niosomes (F1 to F4) were incorporated into the sol–gel system using carbopol-934P (pH-sensitive) and HPMC (viscosity modifier). HPMC serves a dual purpose of decreasing the concentration of carbopol and reducing ocular irritation (Allam et al., 2019). The *in situ* gel-forming systems were formed by adding HPMC (0.8 %; w/v) to 75 % of the aqueous phase, allowing it to hydrate and swell. After that, carbopol (0.2 %; w/v) was dispersed into HPMC solution and allowed to hydrate and swell overnight. The rest of the aqueous vehicle was then gradually added under constant stirring until a uniform solution was achieved. For the purpose of preservation of the formulation, benzalkonium chloride (0.02 % v/v) was mixed with carbopol/HPMC solution.

The niosomes were subjected to cooling ultracentrifugation for 15 min to obtain the pellets, which were then weighed, dissolved, and measured for their ITZ content. The pellets containing an equivalent to 10 mg of ITZ were incorporated into 10 mL *in situ* gel bases, resulting in formation of F1-ISG (F1) to F4-ISG (F4) formulations. The *in situ* gel forming systems were formulated under aseptic conditions.

2.3.1. Evaluation of ITZ-bioadhesive niosomes-laden in situ gels

2.3.1.1. Clarity and pH investigation. The clarity of the formulations was inspected visually under sufficient light to detect any signs of turbidity or the presence of dispersed particles. This visual assessment helps to determine the transparency and homogeneity of the gel. To determine the pH of the gel formulations, an exact amount of gel (2.5 g) was dispersed in 25 ml of distilled water, ensuring proper mixing to obtain a homogeneous dispersion. This step is required to allow the gel to interact with water, providing accurate pH measurement. The pH meter (Mettler Toledo, Greifensee, Switzerland) was immersed in the gel-water mixture, and the pH value was recorded.

2.3.1.2. Gelling capacity determination. The gelling capacity of the *in-situ* gel was determined by mixing the niosomal *in situ* gels with simulated tear fluid (STF) at a pH of 7.4. STF was prepared by dissolving 2 g of $NaHCO_3$, 6.7 g of NaCl, and 0.8 g of $CaCl_2{\cdot}2H_2O$ in 1 L of water. STF mimics the composition of tears under physiological conditions. To mimic the *in vivo* ocular condition, 25 µL of the in-situ gel was mixed with 7 µL of STF. This mixture was then equilibrated at 37 °C, which is the physiological temperature of the eye. The gelation process was visually observed to determine the time needed for gel formation (Adısanoğlu & Özgüney, 2024). The in-situ gel was qualified based on the clarity and maximum gelling capacity.

2.3.1.3. Rheological studies. The viscosity of the obtained gels was determined using a DV-II+, Rotating Brookfield viscometer (Brookfield Engineering Laboratories Inc., Stoughton, MA, USA) with a No. 25 spindle. The shear rate was increased gradually from 5 to 100 rpm. The viscosity was conducted under non-physiological conditions at 25 °C and physiological conditions by adding STF pH 7.4 at 37 °C (Allam et al., 2019). Then, the viscosity values before and after gelation were studied.

2.3.1.4. In vitro release study of ITZ niosomal in situ gels. The *in vitro* release of ITZ from bioadhesive niosomal gel formulations was investigated using Franz diffusion cells with an effective diffusional area of 3.14 cm^2 and 15 mL of receptor compartment capacity. The cellulose membrane (8–14 KDa cut-off) was positioned between the donor and receptor compartments of the diffusion cells. The simulated tear fluid (STF) of pH 7.4 containing TW 80 (0.5 % v/v) was used as the receptor solution and maintained at 37 ± 0.5 °C and 100 rpm via a magnetic stirrer to imitate *in vivo* conditions. The formulations (equivalent to 1 mg of ITZ) were added to the donor compartment. Periodically, 1 mL of the sample was withdrawn at 1, 2, 4, 6, 8, 10, 12, and 24 h and replaced with 1 mL of the receptor media. All samples were filtered through a 0.22 µm pore size cellulose membrane filter and assayed using HPLC. The cumulative amount of ITZ released was calculated as a function of time. Each experiment was carried out in triplicate. The results taken were processed to produce a graph showing the relationship between the percentage of the cumulative ITZ release and time. Furthermore, the kinetic analysis was assessed after fitting the obtained data to different kinetic models, such as Zero-order, First-order, Higuchi diffusion, and Korsmeyer-Peppas models.

2.4. Ex vivo corneal permeation

The *ex vivo* transcorneal permeation of the *in situ* gel formulations and ITZ control was performed using Franz diffusion cell, as previously mentioned. This experiment was carried out according to Guidelines of Research Ethics Committee of King Saud University College of Pharmacy, Riyadh, Saudi Arabia (Ref. No.: KSU-SE-21-71) followed by the National Research Council's Guide for the Care and Use of Laboratory Animals. The male animals were used to reduce the variability and facilitate accurate measurement of corneal permeation for various drugs. The whole eyeballs of the goats (males) were promptly obtained from a local butcher shop and transported to the laboratory in Ringer's salt solution within 1 h of slaughtering (Ahuja et al., 2015). The cornea was precisely excised along with 2–4 mm of surrounding scleral tissues and rinsed with Ringer's salt solution until washing was free from adhering tissues and reserved in freshly prepared STF, pH 7.4 containing TW 80 (0.5 % v/v). The goat cornea was positioned between the donor and receptor compartments of the Franz diffusion cell. The donor compartment was filled with the formulation equivalent to 1 mg of ITZ,

while the receptor compartment was filled with freshly prepared STF (15 mL) and stirred continuously. The epithelial surface of the goat cornea faced the donor compartment. The whole system was maintained at 37 °C to stimulate *in vivo* ocular conditions. Aliquots of 1 mL were withdrawn at various time points of 1, 2, 4, 6, 8, 10, 12, and 24 h and replaced with an equivalent volume of fresh STF solution. All samples were filtered through a 0.22 nm pore size Millipore membrane filter and analyzed using HPLC. Each experiment was carried out in triplicate.

The cumulative ocular permeation profile was conducted by plotting the cumulative amount (Qt) of ITZ (μg/cm^2) vs. time (t). The steady-state flux of FA (*Jss*, μg/cm^2·h) was determined from the slope of the linear portion of the profile, while the X-intercept provided the lag time (TL). The permeability coefficient (*Kp*, cm^2/h) was calculated by dividing the *Jss* by the initial drug concentration (C_0) in the donor compartment. The enhancement ratio (ER) was then obtained by dividing the *Jss* of the respective formulation with *Jss* of control ITZ-ISG (control).

2.5. In vitro antifungal activity

The antifungal activity of ITZ-ISG, F3-ISG, and F4-ISG was evaluated using the agar cup plate method. The microorganisms tested included *Candida albicans (C. albicans), Candida Parapsilosis (C. Parapsilosis), Aspergillus flavus (A. flavus), and Aspergillus Fumigatus (A. Fumigatus)*. Nutrient agar plates were prepared using 30 mL sterilized nutrient agar media inoculated with standard microorganisms (2 mL of inoculums/100 mL of nutrient agar media). In each Petri plate, three wells of 5 mm diameter were created using a sterile borer. An equivalent volume of *in situ* gel containing 5 μg/mL of ITZ was selected based on the previous reports (Permana et al., 2021), and was aseptically transferred to separate wells. Negative and positive controls were also included as un-inoculated media and media containing the test microorganism, respectively. The Petri plates were maintained at room temperature for 2 h to facilitate the diffusion of the solution into the medium and then incubated at 28 °C for 48 h. The diameter of the zone of inhibition was recorded.

2.6. Corneal hydration test

The safety profile of niosomal formulations was investigated through two toxicity studies: a corneal hydration test and histological study (Zubairu et al., 2015). The goat corneas from *ex vivo* permeation studies were used to determine corneal hydration at the end of the permeation examination. Each cornea was weighed, followed by soaking in methanol and drying overnight in an oven at 90 ^{0}C. Afterward, the dried corneas were reweighed. Corneal hydration values were determined by calculating the difference in corneal weights before and after drying.

2.7. Histological study

The excised goat corneas were rinsed with an isotonic NaCL solution (0.9 %, w/v) for 1 min and incubated with selected formulations, negative control (PBS; pH 7.4), and positive control (saturated KCl solution), separately for 1, 6, and 12 h at 37 °C. Following the incubation periods, the corneas were washed with PBS (pH 7.4) and immediately fixed with a 10 % (v/v) formalin solution for 24 h. The corneas were then dehydrated with ethyl alcohol gradient (70 %-90 %-100 %) and xylene. Subsequently, they were embedded in melted paraffin, and allowed to solidify into block forms. The cross-sections (<1 mm) were prepared, mounted on glass slides and stained with hematoxylin and eosin for histological inspection to detect any damage under a microscope (Padmasri & Nagaraju, 2021). This experiment was carried out according to Guidelines of Research Ethics Committee of King Saud University College of Pharmacy, Riyadh, Saudi Arabia (Ref. No.: KSU-SE-21-71).

2.8. Ocular irritation study

Ocular irritation studies were conducted using the Draize test on the cornea of albino rabbits weighing between 2.5–3.5 kg each. The F3-ISG and F3-ISG (2 drops) were instilled into the lower right cul-de-sac of the right eye. In contrast, the left eye received a saline solution (0.9 % NaCL) as a negative control. The other group was treated with sodium lauryl sulfate (1 %) as a positive control. In the absence of irritation, multiple applications were administered three times daily for a duration of 3 days. Throughout the observation period, the rabbits were periodically examined for indications of redness, congestion, and watering of the eyes. The Draize test uses a scoring system that ranges from 0 (no irritation) to 4 (maximum irritation). The test evaluates the cornea for opacity, the iris for inflammation, and conjunctivae for congestion, swelling, and discharge. These procedures were conducted based on a study conducted by Emad Eldeeb et al. 2019 (Emad Eldeeb et al., 2019), and Allam et al. in 2019 (Allam et al., 2019).

2.9. Statistical data analysis

Data analysis was carried out with the software package, Microsoft Excel, Version 2010, and Origin software, Version 8. Results are expressed as mean ± standard deviation (n = 3). A one-way analysis of variance (ANOVA) was performed when comparing three or more conditions ($p < 0.05$).

3. Results and discussion

3.1. Characterization of ITZ loaded-bioadhesive niosomes

3.1.1. Particle size distribution and zeta potential measurements

The particle size, PDI, and zeta potential could affect the performance of ITZ-loaded bioadhesive niosomes in ocular applications. Therefore, they were evaluated to qualify the obtained bioadhesive niosomes. The values of size distribution and zeta potential are represented in Fig. 1 and Table 2. The vesicle sizes of various niosomes were 165.5 ± 3.4 nm for F1, 180.9 ± 5.1 nm for F2, 261.1 ± 9.6 nm for F3, and 378.2 ± 7.2 nm for F4. The magnitude of PDI is used to evaluate the vesicle size distribution, which represents the uniformity of vesicle size. The narrow size distribution is important for enhancing drug absorption (Ameeduzzafar et al., 2020). The niosomes (F1-F4) showed PDI values ranging from 0.194 to 0.362 (Table 2), indicating a relatively homogeneous distribution of vesicle sizes (Khalid et al., 2023).

Zeta potential is an important factor in predicting the physical stability of nanocarriers (Miatmoko et al., 2021). It has been reported that the high value of zeta potential could reduce aggregation during storage, providing long-term stability (Abu El-Enin et al., 2019). ITZ span 60 niosomes (F1) showed a zeta potential of −20.9 ± 2.1, while F2, F3, and F4 had −29.6 ± 3.1, 32.3 ± 1.9, and 22.6 ± 1.3 mV, respectively (Fig. 1 and Table 2).

3.1.2. Entrapment efficiency (EE%)

The EE serves as the main parameter in evaluating the success of niosomal formulations (Verma et al., 2021). The EE% values were 78.1, 84.5, 83.2, and 86.6 % for F1, F2, F3, and F4, respectively (Table 2). The EE% of the bioadhesive niosomes exhibited a significant increase in EE% of ITZ compared to non-bioadhesive ones ($p < 0.05$). However, the EE% between F2, F3, and F4 did not show a significant change in the EE% of ITZ ($p > 0.05$).

3.1.3. Stability study

The stability of bioadhesive niosomes was achieved during 2 months storage period at 4 °C to inspect their stability (Tyagi et al., 2023). The stability data indicated vesicle sizes of 174.8 ± 4.1, 188.1 ± 2.5, 271.6 ± 7.4, and 383.8 ± 5.3 for F1, F2, F3, and F4, respectively, representing that the niosomes remained stable under 4 °C after 2 months. The zeta

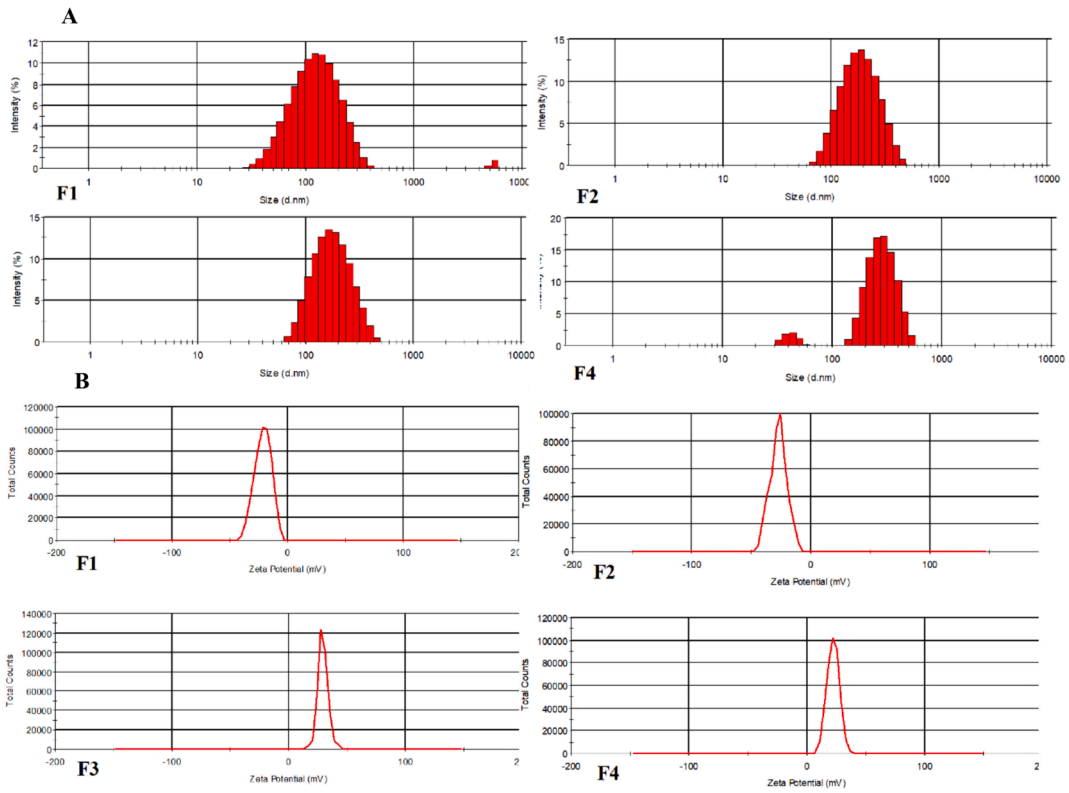

Fig. 1. Particle size distribution (A), and zeta potential (B) of ITZ-loaded bioadhesive niosomes.

Table 2
Particle size, PDI, zeta potential, and entrapment efficiency of ITZ-loaded bioadhesive niosomes.

Formulations	Particle size (nm)	PDI	Zeta potential (mV)	EE%
F1	165.5 ± 3.4	0.194 ± 0.021	−20.9 ± 2.1	78.1 ± 2.2
F2	180.9 ± 5.1	0.318 ± 0.059	−29.5 ± 3.1	84.5 ± 4.1
F3	261.1 ± 9.6	0.362 ± 0.036	32.3 ± 1.9	83.2 ± 3.3
F4	378.2 ± 7.2	0.316 ± 0.031	22.6 ± 2.3	86.6 ± 2.9

potential values were −17.4 ± 1.2, −25.9 ± 2.2, 29.3 ± 7.4, and 20.4 ± 1.6 for F1, F2, F3, and F4, respectively. These results showed an insignificant change in the particle size and zeta potential values ($p > 0.05$) at 4 °C. These slight variations observed were attributed to membrane mobility and permeability, providing additional evidence of the stability of the niosomes (Taymouri & Varshosaz, 2016; Khan et al., 2020; Roque et al., 2020).

3.1.4. Transmission electron microscopy

Fig. 2 displays TEM images of F4, which was selected due to its good value of EE. F1 was also chosen for comparative purposes. TEM images confirmed spherical shapes with a slight aggregation of vesicles. TEM images revealed a smaller vesicle diameter compared to the data obtained by DLS, which can be explained by the dehydration process for TEM observation, whereas the hydration process was used in DLS measurement.

3.2. Itz-bioadhesive niosomes laden-in situ gels

3.2.1. Evaluation of ITZ-bioadhesive niosomes laden-in situ gels

3.2.1.1. Clarity, homogeneity, pH, and gelling capacity. The obtained niosomes, F1, F2, F3, and F4 were incorporated with pH-sensitive *in situ* gels, nominating them as F1-ISG, F2-ISG, F3-ISG, and F4-ISG, respectively. The prepared *in situ* gel formulations were evaluated for their clarity, homogeneity, pH, gelling capacity, and rheology.

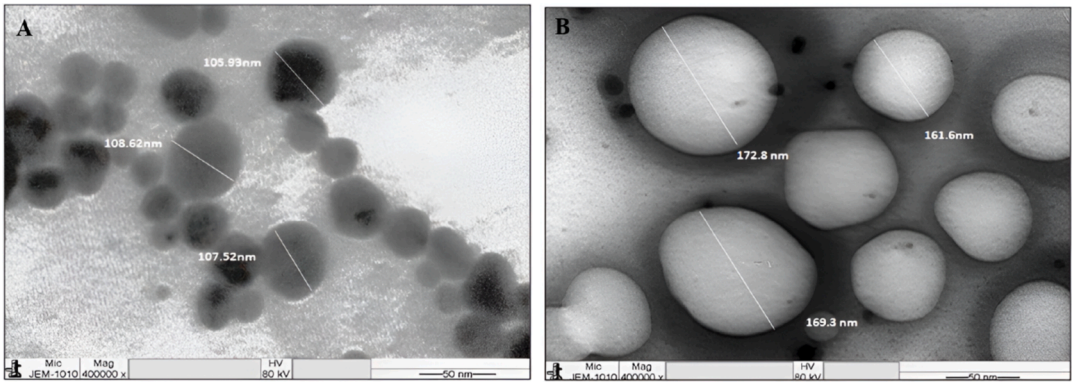

Fig. 2. TEM images of conventional niosomes (F1) and CS-HA double-layer niosomes (F4).

Therefore, F1-ISG, F2-ISG, F3-ISG, and F4-ISG were visually inspected against a black and white background to assess their clarity. They exhibited a semi-transparent appearance with clear homogeneity without any gritty particles (Table 3). Furthermore, pH values were taken at room temperature before gelation and following mixing with STF (pH 7.4) at 37 °C. Firstly, the pH values were between 4.4 and 5.5, which is within the physiologically acceptable range. The presence of carbopol polymer in an ITZ-ISG gel caused a slightly acidic pH (4.8). In the case of F1-ISG and F2-ISG, pH values were 5.43 and 5.44, respectively. However, F3-ISG and F4-ISG formulations (CS) showed a reduction in pH values from 5.43 to 4.54 and 4.65, respectively. The acidic property of the CS-bioadhesive layer may be the reason for the lower pH. Furthermore, pH values of all formulations were increased (~6) by the addition of STF (pH 7.4), which is a suitable pH for ophthalmic use. The gelling capacity was evaluated to measure the duration of gel remaining intact after being exposed to the tear fluid (STF) before its dispersion. Then, these bioadhesive-niosomes laden *in situ* gels offered promising characteristics for potential use in ophthalmology to prolong drug release and contact time with the cornea.

3.2.1.2. Rheological study. The viscosity measurement was done using both non-physiological conditions (initial pH and 25 °C) and physiological conditions (STF, pH 7.4, and 37 °C) (Sheshala et al., 2019). Initially, *in situ* gels showed low viscosity with an increased viscosity after the addition of STF at 37 °C, indicating the conversion of the sol into a gel state. The viscosity values of the *in situ* gel formulations ranged from 1258.9 to 1673.8 mPa·s at 25 °C and increased to approximately 2883.9–3639.3 mPa·s after adding STF at 37 °C (Fig. 3). The level of viscosity values followed the order of ITZ-ISG < F1-ISG < F2-ISG < F3-ISG < F4-ISG, attributed to the bioadhesive layers formed.

The viscosity of bioadhesive niosomes-*in situ* gels was greater compared to normal niosomes-*in situ* gels (F1). The *in situ* gels exhibited non-Newtonian pseudoplastic behavior with a reduced viscosity under higher shear rates (Farooq et al., 2022; Jain et al., 2020).

Fathalla et al. (2022) demonstrated that CS-based *in situ* gels are suitable for ocular uses due to their increased viscosity at the physiological pH of the eye (Fathalla et al., 2022). The increased viscosity makes the formulations more resistant to flow under normal physiological conditions. Importantly, a slight increase in viscosity may be required for ocular application, which improves corneal adherence. These results confirmed the potential application of these *in situ* gels for ocular drug delivery.

3.2.1.3. In vitro release study of ITZ-bioadhesive niosomes-laden in situ gels. The *in vitro* release profiles of the free ITZ (F1-ISG) and ITZ niosomal *in situ* gel formulations are illustrated in Fig. 4. ITZ-ISG, F1-ISG, F2-ISG, F3-ISG, and F4-ISG demonstrated cumulative ITZ release of 21.6 ± 4.1 %, 62.3 ± 3.9 %, 47.7 ± 1.6 %, 41.9 ± 2.8 %, and 33.2 ± 0.8 %, respectively, over 4 h (Fig. 4). After 24 h, the released amounts of ITZ were 45.9 ± 2.8 %, 90.7 ± 3.2 %, 83.7 ± 4.6 %, 80.4 ± 5.2 %, and 76.5 ± 4.7 % for ITZ-ISG, F1-ISG, F2-ISG, F3-ISG, and F4-ISG, respectively. These *in vitro* release profiles exhibited a biphasic pattern with an initial rapid release in the first 4 h, followed by a slow and sustained release over 24 h. The initial burst release of ITZ could be explained by the location of ITZ on the outer surface of the niosomes (Nemr et al., 2022). On the other hand, the release patterns of ITZ from the gel matrix. ITZ-ISG showed a significantly high ITZ release compared to F1-ISG, F2-ISG, F3-ISG, and F4-ISG ($p < 0.05$). F4-ISG displayed the lowest ITZ release significantly ($p < 0.05$), attributed to the extra barrier of the double layer of CS/HA and gel matrix.

Table 3
Clarity, homogeneity, pH, and gelling capacity of ITZ-bioadhesive niosomes laden-*in situ* gels.

In situ gels	Clarity	Homogeneity	pH	Gelling capacity	
			Without STF	With STF	
ITZ-ISG	✓	Good	4.78	6.44	+++
F1-ISG	✓	Good	5.43	6.67	++
F2-ISG	✓	Good	5.44	6.68	+++
F3-ISG	✓	Good	4.54	6.59	+++
F4-ISG	✓	Good	4.65	6.64	+++

F1-ISG: conventional niosomes gel; F2-ISG: HA-bioadhesive niosomes gel; F3-ISG:CS-bioadhesive niosomes gel; F4-ISG: CS/HA-bioadhesive gel.
(+) Gels forms after few min and dissolve quickly.
(++) Immediate gelation that continues for short time (5–10 min).
(+++) Immediate gelation that extends for a long duration (> 2 h).

The result presented in Table 4 showed that the release kinetics of ITZ from bioadhesive niosomal-in *in situ* gels followed Korsmeyer-Peppas model (highest R^2 value). The values of the diffusion exponent (n) were $0.4029 < n < 0.6117$, indicating a non-Fickian diffusion pattern (Heredia et al., 2022). These values of exponent *n* indicate that the release of the drug from the ISG happens mainly through a diffusion mechanism (Ameeduzzafar et al., 2021). The gradual swelling of HA and CS coatings plays a role in the time-dependent effects of the diffusion process (Almalik et al., 2017). The diffusion barriers created by the gel matrix and the coating play a significant role in controlling drug release. In this pattern, the mechanism of drug release is influenced by the combined processes of diffusion and swelling of the gels, as well as the CS, and HA bioadhesive layers of niosomes. Therefore, it is possible to modify the drug release profiles of niosomes for specific therapeutic applications.

3.3. Ex vivo corneal permeation study

The profiles of the *ex vivo* corneal permeation of bioadhesive niosomes-laden pH sensitive *in situ* gels are presented in Fig. 5. The permeated amounts of ITZ were 87.5 ± 6.4 μg/cm^2, 112.4 ± 5.3 μg/cm^2, 138.4 ± 7.1 μg/cm^2, 191.2 ± 6.6 μg/cm^2, and163.0 ± 7.8 for ITZ-ISG, F1-ISG, F2-ISG, F3-ISG, and F4-ISG, respectively.

The significant amounts of permeated ITZ from F3-ISG and F4-ISG were detected compared to other formulations ($p < 0.05$). Table 5 displays the permeation parameters, including *Jss, Kp,* and TL. It was indicated that the difference in the permeation parameters of ITZ from bioadhesive niosomes-laden ISG was significantly influenced by their composition. The high permeation parameters of F3-ISG could be attributed to the good bioadhesive properties of CS (Karuppaiah et al., 2020). The highest J_{SS} value (8.04 ± 0.11 μg/cm^2/h) of F3-ISG was approximately 2.10 times greater than that of F1-ISG ($p < 0.05$). Furthermore, the *Kp* value of F3-ISG was significantly higher ($P < 0.05$) in comparison to F1-ISG (Table 5) with a T_L of 2 h. The greater permeation of bioadhesive niosomes-laden into bioadhesive gels can be attributed to the presence of surfactant (span 60), lipid, nanosized-vesicles, and bioadhesive polymers (HA/CS) (Jeon et al., 2015). This significant permeation may result from the formation of a gel over the corneal layer, allowing controlled ITZ release (Ameeduzzafar et al., 2021). Moreover, the nanoscaled-vesicles in niosomes facilitate the corneal uptake through receptor-medited endocytosis, while the bioadhesive and penetrating properties of CS and FA contribute to higher permeation (Valachová & Šoltés, 2021).

3.4. In vitro antifungal activity

The *in vitro* antifungal efficacy of the bioadhesive-ITZ niosomal-laden *in situ* gels (ITZ-ISG, F3-ISG, and F4-ISG) was assessed by the agar-cup diffusion assay. This study was performed on yeasts such as *C. Albicans* and *C. Parapsilosis*, as well as molds including *A. Flavus* and A. *Fumigatus*. The zone of inhibition was displayed in Fig. 6. ITZ-ISG exhibited a zone of inhibition of 7.1 ± 0.61, 9.0 ± 0.50, 6.0 ± 0.51, and 9.0 ± 0.70, against *C. Albicans*, *C. Parapsilosis, A. Flavus, and A. Fumigatus,* respectively. F3-ISG exhibited a zone of inhibition of 16.01 ± 1.01, 23.0 ± 1.25, 13.0 ± 1.11, and 15.0 ± 0.95, against *C. Albicans*,

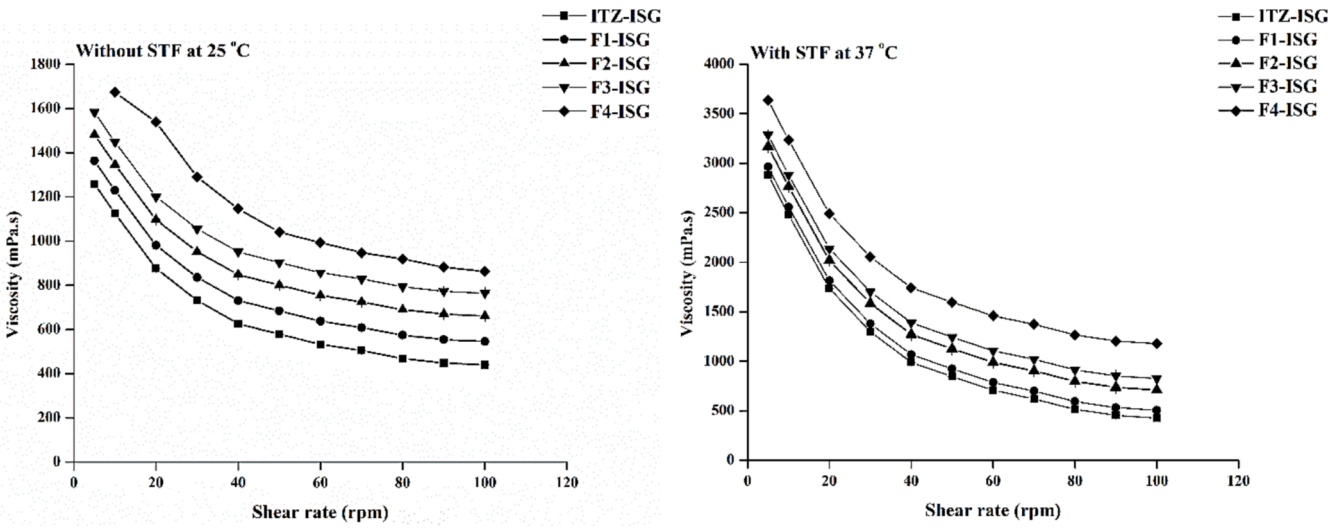

Fig. 3. Viscosity at 25 °C without STF and 37 °C with STF of ITZ loaded bioadhesive niosomes-laden *in situ* gel systems.

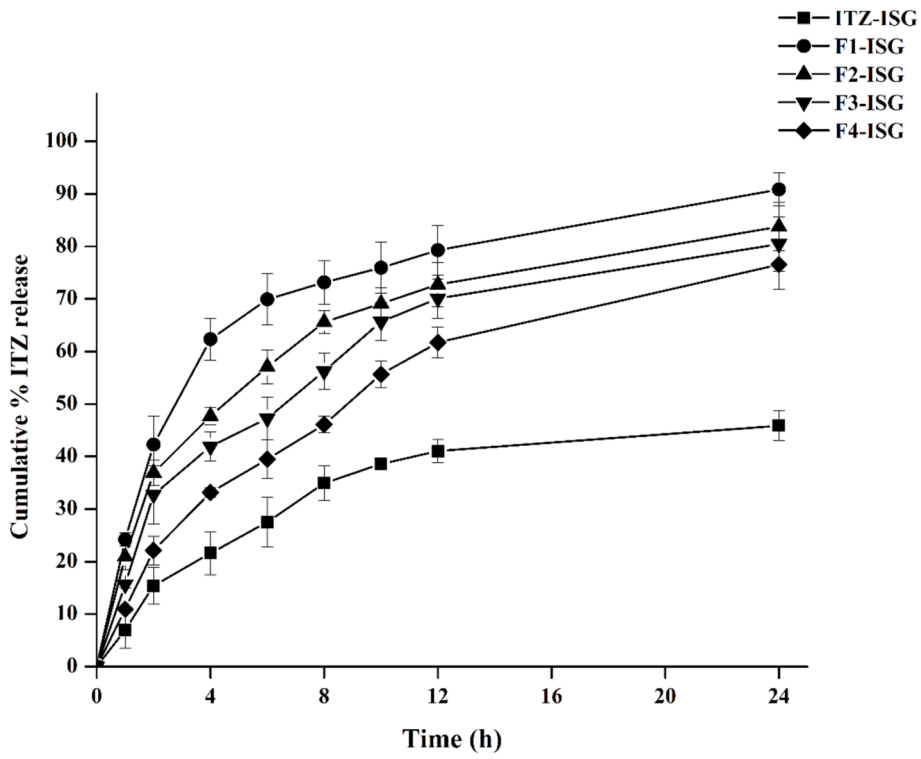

Fig. 4. *In vitro* release profile of ITZ loaded bioadhesive niosomes-laden *in situ* gels.

Table 4
In vitro release kinetics model of niosomal *in situ* gel formulations.

Formulations	Zero order	First order	Higuchi	Hixon Crowell	Korsmeyer-Peppas	n value
ITZ-ISG	0.7519	0.8065	0.9107	0.7862	0.9380	0.599
F1-ISG	0.6318	0.9034	0.8530	0.8531	0.9021	0.4029
F2-ISG	0.7097	0.9056	0.9189	0.8775	0.9496	0.4337
F3-ISG	0.7606	0.9189	0.9342	0.8912	0.9391	0.5003
F4-ISG	0.8519	0.9624	0.9725	0.9398	0.9736	0.6117

C. Parapsilosis, A. Flavus, and A. Fumigatus, respectively. Whereas, F4-ISG exhibited a zone of inhibition of 10.01 ± 1.12, 17.0 ± 1.00, 10.0 ± 0.65, and 11.0 ± 0.80, against *C. Albicans*, *C. Parapsilosis, A. Flavus, and A. Fumigatus,* respectively. A significant difference ($p < 0.05$) was noticed between the values of the inhibition zones between ITZ-ISG, F3-ISG, and F4-ISG. The antifungal efficiency was higher in F3-ISG, followed by F4-ISG, and lowest in ITZ-ISG.

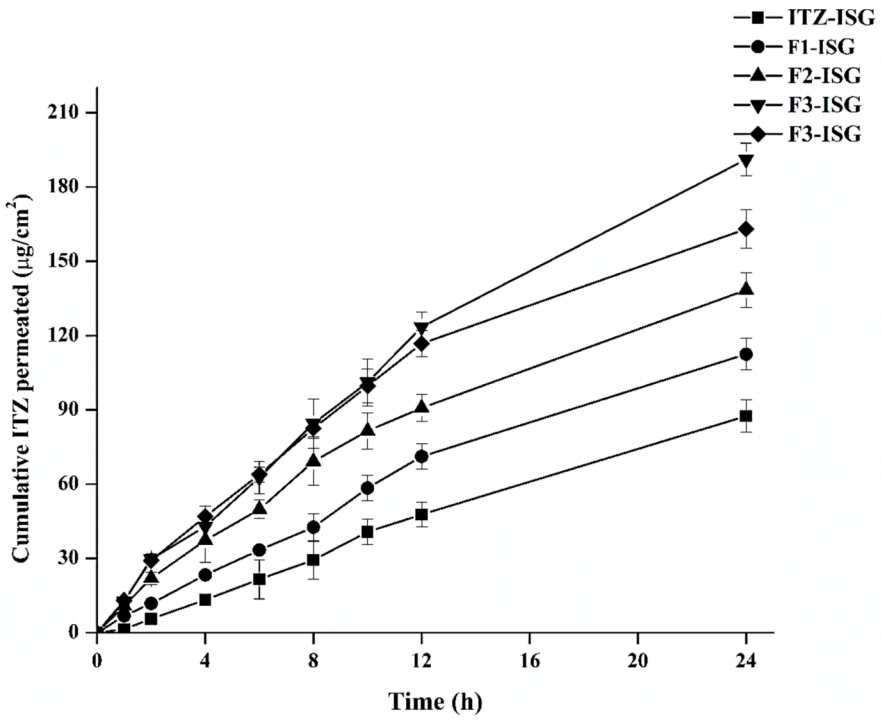

Fig. 5. *Ex vivo* permeation of ITZ loaded bioadhesive niosomes-laden *in situ* gels.

Table 5
Ex vivo permeation parameters of ITZ loaded bioadhesive niosomes-laden *in situ* gels.

Formula codes	Flux, J (μg/cm²/h)	Permeability coefficient Kp*10⁻³ (cm h⁻¹)	Lag time (T_L h)	Enhancement ratio (ER)
ITZ-ISG	3.83 ± 0.28	3.84 ± 0.13	0.53 ± 0.19	–
F1-ISG	4.80 ± 0.13	4.80 ± 0.14	1.17 ± 0.55	0.97
F2-ISG	5.90 ± 0.15	5.88 ± 0.06	2.82 ± 0.58	1.54
F3-ISG	8.04 ± 0.11	8.04 ± 0.03	1.98 ± 0.30	2.10
F4-ISG	6.86 ± 0.26	6.90 ± 0.24	3.32 ± 0.13	1.78

3.5. Corneal hydration test

The corneal hydration test is usually used to measure the degree of corneal tissue damage (Dubashynskaya et al., 2019). The normal range of corneal hydration is 76–80 %; a level higher than 83 % indicates damage to the epithelium and/ or endothelium of the cornea (Dubashynskaya et al., 2019). Following the application of bioadhesive niosomes-laden *in situ* gels (F3-ISG and F4-ISG, high antifungal activity), the corneal hydration levels were within the normal range (76–77.5 %). This indicates that the cornea did not change during the duration of the study (Ahmed et al., 2023). It has been reported that if a level of corneal hydration is more than 83 %, damage to the cornea is observed (Pramanik et al., 2021). Consequently, the obtained formulations were safe for ocular application.

3.6. Histological study

The histological study of the cornea structure was conducted to check the safety of F3-ISG and F4-ISG (high antifungal activity) by investigating for any abnormalities in both the epithelium and stroma layers (Pramanik et al., 2020). The obtained findings showed a remarkable absence of any unfavorable defects on the corneal surfaces after applying formulations and NaCL 0.9 % w/v. On the contrary, KCl solution (positive control) demonstrated clear damage to the corneal tissues (Fig. 7). The F3-ISG and F4-ISG formulations did not show a significant effect on the cornea's structure with an intact epithelial layer without signs of inflammation in the stroma. There were no signs of tissue abnormalities, such as corneal epithelium rem loss or cell necrosis.

3.7. Eye irritation study

The irritation of the eye is a common problem in ophthalmic preparation that can affect patient compliance (Badran et al., 2022). Based on the antifungal activity, F3-ISG and F4-ISG were selected for ocular irritation. The rabbits' eyes were periodically observed for signs of redness, swelling, and tear production (Karuppaiah et al., 2020). After administration of positive control, ocular irritancy was noticed (redness, increased tear, and inflammation). However, slight redness after application of F3-ISG and F4-ISG was detected and disappeared within 2 h. It has been reported that CS-bioadhesive nanocarriers laden into *in situ* gels exhibited their potential to safely deliver many drugs such as metronidazole, chlorhexidine, or nystatin loaded against fungal infections (Valachová & Šoltés, 2021). Thus, F3-ISG and F4-ISG were non-irritating and safe for ophthalmic application. Further preclinical studies are necessary to assess the safety and efficacy of F3-ISG and F4-ISG for ocular applications.

4. Discussion

The main goal of the current study was to explore the effectiveness of bioadhesive niosomes for ocular delivery of ITZ. These niosomes can enhance the drug ocular permeation based on the presence of nonionic surfactants like span 60 and phospholipids (Khatoon et al., 2017). Furthermore, they were coated by biopolymers, specifically CS and HA, to improve their bioadhesiveness properties (Zhang et al., 2021; Badran et al., 2022). These natural polymers were selected for their biocompatibility, biodegradability, biological activity, and CD44 receptors targetability, which are expressed on ocular tissues (Zhang et al., 2021).

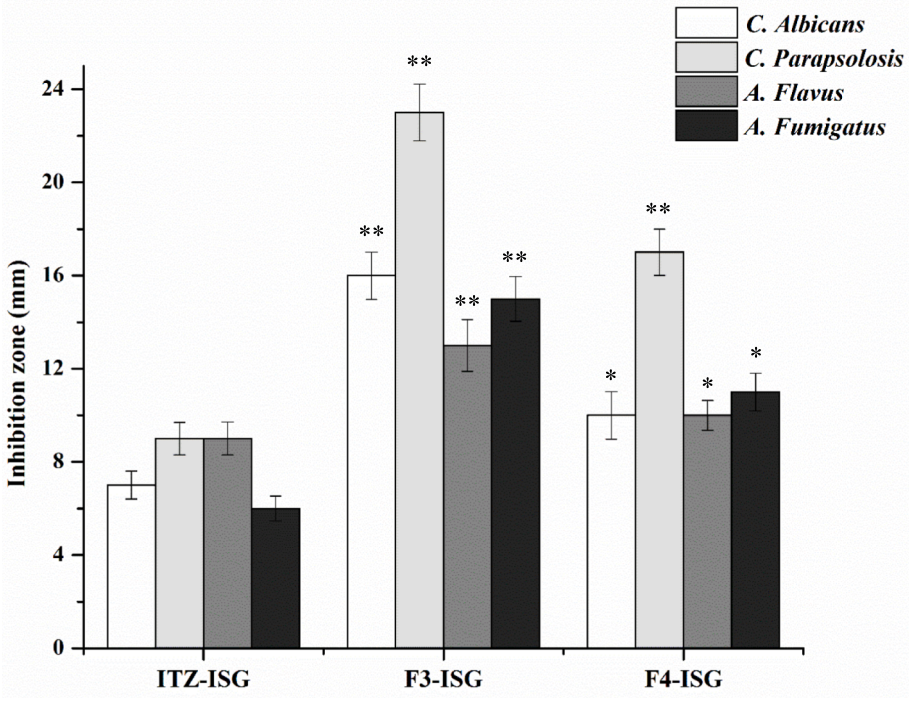

Fig. 6. Antifungal activity of ITZ-ISG, F3-ISG, and F4-ISG using cup plate method (inhibition zone in mm ± SD). Statistical analysis was performed based on one-way ANOVA for data from F2-ISG and F4-ISG compared to ITZ-ISG (control). The p-values are indicated by stars, ** $p < 0.05$ (N = 3).

The proniosomes were firstly formulated using the coacervation phase separation technique (Darson et al., 2023). The resultant proniosomes exhibited a uniform semisolid-creamy consistency, which upon hydration converted into niosomes. This strategy provides a simple method for niosome formation with numerous advantages, such as high stability, scalability, and more drug loading capacity. The surface of the formed niosome can be further modified by coating them with CS and HA through electrostatic interactions, thereby augmenting their efficiency for ocular applications (Hintze et al., 2022).

The niosomes were categorized as conventional niosomes (F1), bioadhesive niosomes with HA (F2), and CS (F3), and bi-layered using CS/HA (F4). The F1 formulation showed a small vesicle size, which may be attributed to the low HLB value of span 60 (4.7). Span 60 is a hydrophobic surfactant that forms small bilayers due to its arrangement in the vesicle structure to reduce surface free energy (El-Emam et al., 2023). This finding is also consistent with previous studies on paclitaxel niosomes (Bayindir & Yuksel, 2010) and ellagic acid niosomes (Junyaprasert et al., 2012). Furthermore, the vesicle size of bioadhesive niosomes was increased because of the coating layer, such as HA, CS, or both. The increased vesicle size indicates the successful presence of a coating layer on the niosomal surface. It was detected that the size of the HA-bioadhesive niosomes (F2) was smaller than that of the CS-bioadhesive niosomes (F3). The small molecule and low molecular weight of HA (F2) result in a smaller vesicle size than in the F3 (Nemr et al., 2022). In addition, HA has hydrophilic properties that create a tight thin layer around the niosomes. The large vesicle size of F3 may be related to the greater viscosity of CS deposit layer (Ameeduzzafar et al., 2020). Moreover, the double-layered CS/HA-bioadhesive niosomes (F4) had the largest vesicle size. This behavior is due to the electrostatic interaction between the positively charged amino groups of CS and the negatively charged carboxyl groups of HA causing a double-layered coating (Yoo et al., 2016).

The variations in zeta potential values were observed, which may confirm the presence of a coating layer around the bioadhesive niosomes (F2, F3, and F4). The negative zeta potential detected in F1 was attributed to the presence of negatively charged phosphate groups in phospholipids, while span 60 could absorb hydroxyl ions from the surrounding aqueous phase (Darson et al., 2023). However, the high negative zeta potential of F2 is primarily due the anionic property of HA, which outcomes from the deprotonation of the carboxyl groups at pH 7.4 (Hanieh et al., 2021). Furthermore, phospholipid could attach to HA by hydrogen bonds, due to their presence of amide, hydroxyl, and carboxyl groups (Hanieh et al., 2021). The more negative zeta potential value observed for F2 indicates the successful coating of niosomes with HA. The positive zeta potential of F3 revealed the successful formation of a CS-bioadhesive layer on the surface of niosomes, attributed to the existence of amine groups (Pourseif et al., 2023). In the case of F4, double-layer bioadhesive niosomes (HA and CS) had positive zeta potential values (22.6 ± 2.3), owing to the outermost CS layer on niosomes. This value proposes the balance of positive and negative charges from the CS and HA layers. The differences in zeta potential values clearly revealed the successful coating to the surface of niosomes. The obtained niosomes display characteristics that make them suitable for ocular applications due their small size and surface properties, thereby facilitating the interaction with the ocular mucosa depending on the effect of HA/CS.

The EE of niosomes was influenced by surfactant type, presence of phospholipids, cholesterol, and coating layer. These high values of EE are due to the formation of an increased number of proniosomal vesicles with a hydrophobic property of span 60 (Darson et al., 2023). The long alkyl chain, a gel transition temperature of 56 to 58 °C, and an HLB value of 4.7 of span 60 can raise the EE% for many drugs (Durak et al., 2020). Moreover, the hydrophobic nature of both span 60 and ITZ may promote high interactions for efficient entrapment (Durak et al., 2020). The formation of multilayered hydrophobic bilayers (MLVs) can result in niosomes with a higher EE% for hydrophobic drugs. The cholesterol was added to prevent the leaking of the entrapped drug, which further increases EE% (Verma et al., 2021). Moreover, the bioadhesive-niosomes with HA or CS resulted in slightly increased values of EE compared to F1 (conventional niosomes), due to the change in surface properties after coating. The high EE may be due to the interaction between polymers and drugs in solution (Sebaaly et al., 2021; Khallaf et al., 2020).

This study proposed that the bioadhesive niosomal-laden pH

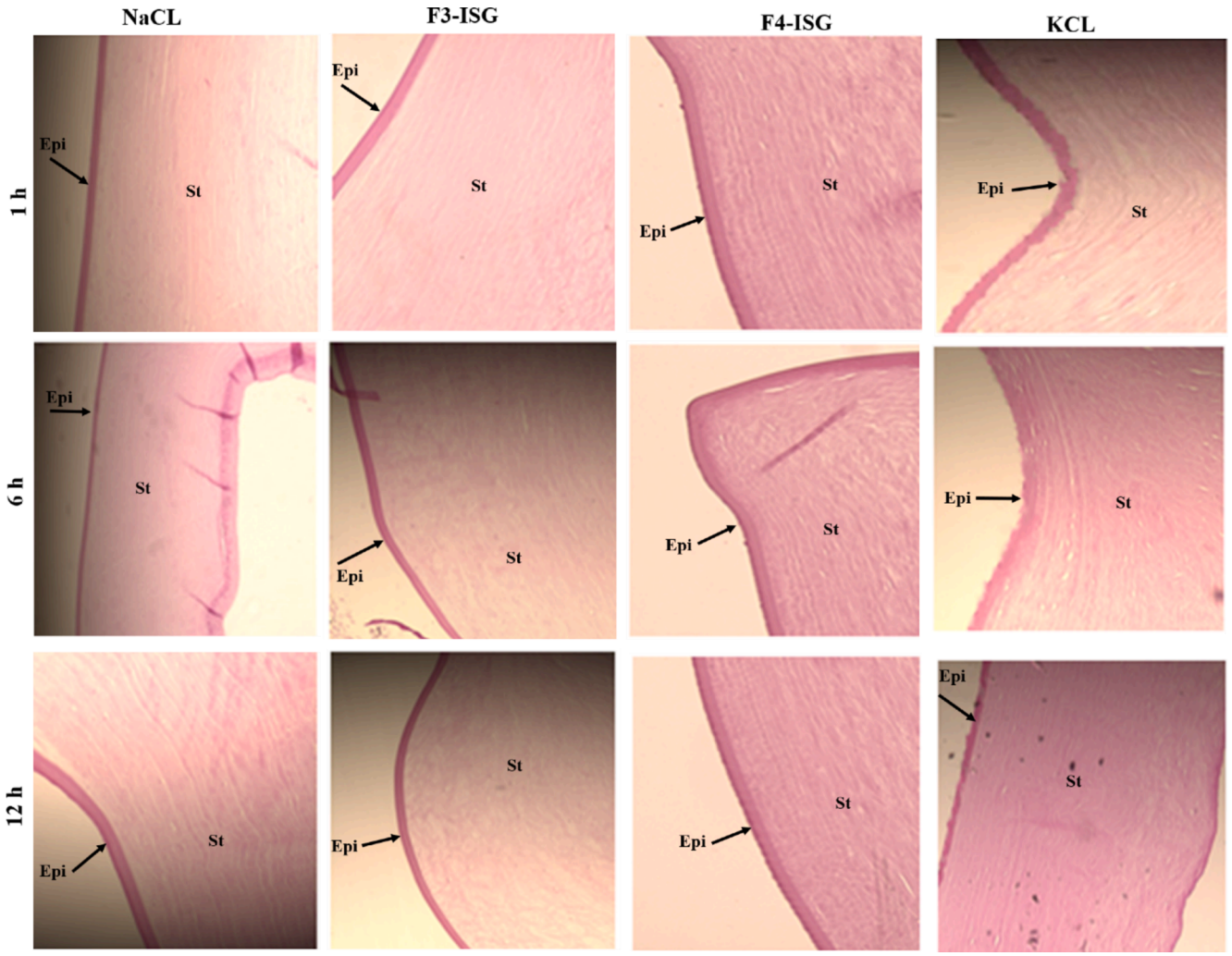

Fig. 7. Histological images of cornea after incubation with *in* ITZ-bioadhesive niosomes laden-*in situ* gels; F3-ISG and F4-ISG.

sensitive-*in situ* gel was anticipated to further increase the duration of residency and improve the therapeutic outcomes, thereby boosting the ophthalmic availability of the drugs. pH sensitive *in situ* gel system is easily administered as drops, which were the converted into a gel state at the application site. This transformation could improve ocular availability, resulting in a reduction of frequent administration (Gugleva et al., 2019; Karuppaiah et al., 2020). The obtained *in situ* gels were converted into gel after contact with STF immediately, which extends for a long duration. This could prolong the contact time between the drug and cornea, facilitating ITZ permeation (Karuppaiah et al., 2020). These *in situ* gel solution have a proper viscosity to drop it easily into the eyes (Sheshala et al., 2019; Karuppaiah et al., 2020).

The presence of a bioadhesive layer had a great impact on the release profiles of the dugs (Ameeduzzafar et al., 2020). In addition, the low *in vitro* release of ITZ profiles after incorporation of niosomes with *in situ* gels was detected. This behavior could be attributed to the viscosity of the obtained gels, which provides an additional barrier for ITZ release (Fathalla et al., 2022). The presence of a bioadhesive layer could hamper the release of ITZ from the vesicular systems due to steric hindrance (Khallaf et al., 2020). The highest ITZ release was observed with conventional niosomes. While, the bioadhesive niosomes-*in situ* gels exhibited a rapid release of ITZ within the first 4 h followed by a sustained release of ITZ up to 24 h. The lowest released rate of ITZ was detected in F3-ISG and F4-ISG, which could be attributed to the coating layers of CS and HA. Furthermore, CS/HA layer and *in situ* gel (F4-ISG) may increase the thickness of the bioadhesive layer of the niosomes, resulting in a further retardation of ITZ release meaningfully.

It has been known that HA and CS are effective polymers that are frequently used in ocular applications (Puluhulawa et al., 2022). HA has ability to bind to mucin and interact with CD44 receptors on the surface of ocular cells, providing ocular absorption (Zhang et al., 2021). CS could increase the ocular permeability due to different mechanisms, such as interactions with the negatively charged surface, a tight junction opening, and mucin binding. They significantly enhanced the permeation of ITZ compared to its control due to their nanoscale size. Additionally, the bioadhesive-niosomes laden-*in situ* gels exhibited higher corneal permeation. Among the bioadhesive formulations, the niosomes with layer-by-layer CS-bioadhesive (F3-ISG) displayed the maximum permeation of ITZ. Furthermore, F4-ISG formulation demonstrated higher permeation compared to F2-ISG. This could be attributed to the magnitude of positively charged niosomes, which facilitate the interaction with the corneal surface. As well, CS with *in situ* gelling systems has excellent mucoadhesive properties, which promote ocular drug permeation (Karuppaiah et al., 2020). Elkomy et al. (2022) showed an increase in flurbiprofen corneal absorption with a safety profile after the use of CS-bioadhesive liposomes (Elkomy et al., 2022). Miatmoko et al., 2021 confirmed the enhanced therapeutic outcome of ursolic acid by using CS-bioadhesive niosomes (Miatmoko et al., 2021). These findings indicated that the *in situ* gels containing bioadhesive niosomes with HA (F2-ISG), CS (F3-ISG), and CS/HA (F4-ISG) could be advantageous for ocular applications and therapeutic effects. This behavior leads to a more pronounced effect on the cornea area for better management of

fungal infections. Furthermore, the enhancement in the antifungal efficiency of F3-ISG was observed. The positive charge of CS enables ITZ to enter the fungal cells by electrostatic interactions between the positively charged CS and the negatively charged fungal cell membranes (Guarnieri et al., 2022). The formulations F3-ISG presented a higher zone of inhibition against *A. Parapsilosis (*23.0 ± 1.22, $p < 0.05$), indicating that CS could potentially address the issue of antifungal resistance in certain strains of *C. Parapsilosis* (Hemmingsen et al., 2021). CS-bioadhesive nanoparticles containing fluconazole exhibited a considerably lower burden of *C. albicans* compared to fluconazole alone (Hemmingsen et al., 2021). In addition, the boosted therapeutic effect of clotrimazole-niosomes-laden *in situ* gel could be ascribed to the high mucoadhesion (Ning et al., 2005). The effectiveness of terbinafine hydrochloride-loaded niosomal *in situ* gel against the treatment of fungal nail infections was augmented (Hassan et al., 2023). The corneal hydration, histological, and irritation evaluation indicates that F3-ISG and F4-INS do not impact cornea tissue, revealing the biocompatibility and safety of the developed bioadhesive niosomal gels. Therefore, these formulations could represent a promising approach to the treatment of ocular fungal infections.

5. Conclusion

The ITZ-loaded bioadhesive niosomes were successfully formulated at the nanoscale, demonstrating spherical shapes. Furthermore, the bioadhesive niosomes displayed distinct features due to the increased vesicle sizes, ranging from 165.5 ± 3.4 to 378.2 ± 7.2 nm and variations in zeta potential values within -20.9 ± 2.1 (F1, conventional niosomes), -29.5 ± 3.1 (F2, HA-coating), 32.3 ± 1.9 (F3, CS-coating), and 22.6 ± 1.3 mV (F4, CS/HA/coating). This behavior confirmed the successful HCS and HA coating. These coating layers had a favorable effect on the EE%, reaching up to 86.6 ± 2.9 %, and enhanced ITZ release profiles of ITZ, achieving the range of 80.4 ± 5.2 % to 90.7 ± 3.2 % at 24 h. Moreover, these bioadhesive niosomes were incorporated into pH sensitive *in situ* gels proving proper pH values, excellent gelling capacity, and suitable viscosity. *Ex vivo* transcorneal permeation revealed that F3-ISG and F4-ISG showed the highest flux than F2-ISG and ITZ-ISG (control). As well, they had remarkable antifungal efficacy against various fungal strains based on the high values of zone of inhibition compared to the other formulations ($p < 0.05$). The corneal hydration, irritation, and histopathology results in a noticeable safety effect. These data revealed the potential uses of CS-bioadhesive niosomes-laden *in situ* gels as a promising strategy to improve the delivery of ITZ for the effective management of ocular fungal infections.

CRediT authorship contribution statement

Mohamed M. Badran: Writing – review & editing, Writing – original draft, Supervision, Methodology, Investigation, Formal analysis, Data curation, Conceptualization. **Areej Alsubaie:** Writing – review & editing, Writing – original draft, Methodology, Investigation, Data curation. **Mounir M. Salem Bekhit:** Investigation, Methodology, Writing – original draft, Writing – review & editing. **Abdullah H. Alomrani:** Writing – review & editing, Writing – original draft, Formal analysis. **Aliyah Almomen:** Visualization, Methodology, Investigation. **Mohamed Abbas Ibrahim:** Writing – review & editing. **Doaa Hasan Alshora:** Writing – review & editing.

Funding

This work was funded by the Researchers Supporting Project number (RSPD2023R1008), King Saud University, Riyadh, Saudi Arabia.

Declaration of competing interest

The authors declare that they have no known competing financial interests or personal relationships that could have appeared to influence the work reported in this paper.

Acknowledgments

The authors extend their appreciation to the Researchers Supporting Project number (RSPD2024R1008), King Saud University, Riyadh, Saudi Arabia.

Appendix A. Supplementary material

Supplementary data to this article can be found online at https://doi.org/10.1016/j.jsps.2024.102208.

References

Abu El-Enin, A.S., Khalifa, M.K., Dawaba, A., Dawaba, H., 2019. Proniosomal gel-mediated topical delivery of fluconazole: Development, in vitro characterization, and microbiological evaluation. J. Adv. Pharm. Technol. Res. 10 (1), 20. https://doi.org/10.4103/japtr.JAPTR_332_18.

Adısanoğlu, P., Özgüney, I., 2024. Development and characterization of thermosensitive and bioadhesive ophthalmic formulations containing flurbiprofen solid dispersions. Gels 10 (4), 267. https://doi.org/10.3390/gels10040267.

Ahmed, S., Amin, M.M., Sayed, S., 2023. Ocular drug delivery: a comprehensive review. AAPS PharmSciTech 24 (2), 66. https://doi.org/10.1208/s12249-023-02516-9.

Ahuja, M., Verma, P., Bhatia, M., 2015. Preparation and evaluation of chitosan–itraconazole co-precipitated nanosuspension for ocular delivery. J. Exp. Nanosci. 10 (3), 209–221. https://doi.org/10.1080/17458080.2013.822108.

Ajrin, M., Anjum, F., 2022. Proniosome: a promising approach for vesicular drug delivery. Turkish J. Pharm. Sci. 19 (4), 462–475. https://doi.org/10.4274/tjps.galenos.2021.53533.

Alhowyan, A.A., Altamimi, M.A., Kalam, M.A., Khan, A.A., Badran, M., Binkhathlan, Z., Alkholief, M., Alshamsan, A., 2019. Antifungal efficacy of Itraconazole loaded PLGA-nanoparticles stabilized by vitamin-E TPGS: In vitro and ex vivo studies. J. Microbiol. Methods 161, 87–95. https://doi.org/10.1016/j.mimet.2019.01.020.

Allam, A., El-Mokhtar, M.A., Elsabahy, M., 2019. Vancomycin-loaded niosomes integrated within pH-sensitive in-situ forming gel for treatment of ocular infections while minimizing drug irritation. J. Pharm. Pharmacol. 71 (8), 1209–1221. https://doi.org/10.1111/jphp.13106.

Almalik, A., Benabdelkamel, H., Masood, A., Alanazi, I.O., Alradwan, I., Majrashi, M.A., Alfadda, A.A., Alghamdi, W.M., Alrabiah, H., Tirelli, N., Alhasan, A.H., 2017. Hyaluronic acid coated chitosan nanoparticles reduced the immunogenicity of the formed protein corona. Sci. Rep. 7 (1), 10542. https://doi.org/10.1038/s41598-017-10836-7.

Alomrani, A.H., Al-Agamy, M.H., Badran, M.M., 2015. In vitro skin penetration and antimycotic activity of itraconazole loaded niosomes: Various non-ionic surfactants. J. Drug Delivery Sci. Technol. 28, 37–45. https://doi.org/10.1016/j.jddst.2015.04.009.

Alshora, D., Ibrahim, M., Alanazi, N., Alowyid, M., Ali Alnakhli, Z., Mohammed Alshiban, N., Maodaa, S., Alyami, N.M., Alotaibi, I., 2023. Formulation of Glibenclamide proniosomes for oral administration: Pharmaceutical and pharmacodynamics evaluation. Saudi Pharm. J. 31 (12), 101830. https://doi.org/10.1016/j.jsps.2023.101830.

Ameeduzzafar, Q.M., Alruwaili, N.K., et al., 2021. BD-based development of itraconazole loaded nanostructured lipid carrier for topical delivery: in vitro evaluation and antimicrobial assessment. J. Pharm. Innov. 16, 85–98.

Ameeduzzafar, A.N.K., Imam, S.S., Alotaibi, N.H., Alhakamy, N.A., Alharbi, K.S., Alshehri, S., Afzal, M., Alenezi, S.K., Bukhari, S.N.A., 2020. Formulation of chitosan polymeric vesicles of ciprofloxacin for ocular delivery: box-behnken optimization, in vitro characterization, HET-CAM irritation, and antimicrobial assessment. AAPS PharmSciTech 21 (5), 167. https://doi.org/10.1208/s12249-020-01699-9.

Badran, M.M., Alomrani, A.H., Almomen, A., Bin Jardan, Y.A., Abou El Ela, A.E.S., 2022. Novel metoprolol-loaded chitosan-coated deformable liposomes in thermosensitive in situ gels for the management of glaucoma: a repurposing approach. Gels 8 (10), 635. https://doi.org/10.3390/gels8100635.

Bayindir, Z.S., Yuksel, N., 2010. Characterization of niosomes prepared with various nonionic surfactants for paclitaxel oral delivery. J. Pharm. Sci. 99 (4), 2049–2060. https://doi.org/10.1002/jps.21944.

Bhattacharjee, A., Das, P.J., Adhikari, P., Marbaniang, D., Pal, P., Ray, S., Mazumder, B., 2019. Novel drug delivery systems for ocular therapy: With special reference to liposomal ocular delivery. Eur. J. Ophthalmol. 29 (1), 113–126. https://doi.org/10.1177/1120672118769776.

Bongomin, F., Gago, S., Oladele, R., Denning, D., 2017. Global and multi-national prevalence of fungal diseases-estimate precision. J. Fungi 3 (4), 57. https://doi.org/10.3390/jof3040057.

Darson, J., Thirunellai Seshadri, R., Katariya, K., Mohan, M., Srinivas Kamath, M., Etyala, M.A., Chandrasekaran, G., 2023. Design development and optimisation of multifunctional Doxorubicin-loaded Indocynanine Green proniosomal gel derived niosomes for tumour management. Sci. Rep. 13 (1), 1697. https://doi.org/10.1038/s41598-023-28891-8.

Dubashynskaya, N., Poshina, D., Raik, S., Urtti, A., Skorik, Y.A., 2019. Polysaccharides in ocular drug delivery. Pharmaceutics 12 (1), 22. https://doi.org/10.3390/pharmaceutics12010022.

Durak, S., Esmaeili Rad, M., Alp Yetisgin, A., Eda Sutova, H., Kutlu, O., Cetinel, S., Zarrabi, A., 2020. Niosomal drug delivery systems for ocular disease-recent advances and future prospects. Nanomaterials 10 (6), 1191. https://doi.org/10.3390/nano10061191.

El-Emam, G.A., El-Baz, A.M., Shata, A., Shaaban, A.A., Adel El-Sokkary, M.M., Motawea, A., 2023. Formulation and microbiological ancillary studies of gemifloxacin proniosomes for exploiting its role against LPS acute pneumonia model. J. Drug Delivery Sci. Technol. 81, 104053. https://doi.org/10.1016/j.jddst.2022.104053.

Elkomy, M.H., Ali, A.A., Eid, H.M., 2022. Chitosan on the surface of nanoparticles for enhanced drug delivery: A comprehensive review. J. Control. Release 351, 923–940. https://doi.org/10.1016/j.jconrel.2022.10.005.

Emad Eldeeb, A., Salah, S., Ghorab, M., 2019. Proniosomal gel-derived niosomes: An approach to sustain and improve the ocular delivery of brimonidine tartrate; formulation, in-vitro characterization, and in-vivo pharmacodynamic study. Drug Deliv. 26 (1), 509–521. https://doi.org/10.1080/10717544.2019.1609622.

Farooq, M., Usman, F., Zaib, S., Shah, H.S., Jamil, Q.A., Akbar Sheikh, F., Khan, A., Rabea, S., Hagras, S.A.A., El-Saber Batiha, G., Khan, I., 2022. Fabrication and evaluation of voriconazole loaded transethosomal gel for enhanced antifungal and antileishmanial activity. Molecules 27 (10), 3347. https://doi.org/10.3390/molecules27103347.

Fathalla, Z., Mustafa, W.W., Abdelkader, H., Moharram, H., Sabry, A.M., Alany, R.G., 2022. Hybrid thermosensitive-mucoadhesive in situ forming gels for enhanced corneal wound healing effect of L-carnosine. Drug Deliv. 29 (1), 374–385. https://doi.org/10.1080/10717544.2021.2023236.

Ge, X., Wei, M., He, S., Yuan, W.-E., 2019. Advances of non-ionic surfactant vesicles (niosomes) and their application in drug delivery. Pharmaceutics 11 (2), 55. https://doi.org/10.3390/pharmaceutics11020055.

Gharbavi, M., Amani, J., Kheiri-Manjili, H., Danafar, H., Sharafi, A., 2018. Niosome: A promising nanocarrier for natural drug delivery through blood-brain barrier. Adv. Pharmacol. Sci. 2018, 1–15. https://doi.org/10.1155/2018/6847971.

Guarnieri, A., Triunfo, M., Scieuzo, C., Ianniciello, D., Tafi, E., Hahn, T., Zibek, S., Salvia, R., De Bonis, A., Falabella, P., 2022. Antimicrobial properties of chitosan from different developmental stages of the bioconverter insect Hermetia illucens. Sci. Rep. 12 (1), 8084. https://doi.org/10.1038/s41598-022-12150-3.

Gugleva, V., Titeva, S., Rangelov, S., Momekova, D., 2019. Design and in vitro evaluation of doxycycline hyclate niosomes as a potential ocular delivery system. Int. J. Pharm. 567, 118431. https://doi.org/10.1016/j.ijpharm.2019.06.022.

Hanieh, P.N., Forte, J., Di Meo, C., Ammendolia, M.G., Del Favero, E., Cantù, L., Rinaldi, F., Marianecci, C., Carafa, M., 2021. Hyaluronic acid derivative effect on niosomal coating and interaction with cellular mimetic membranes. Molecules 26 (11), 3434. https://doi.org/10.3390/molecules26113434.

Hassan, S.U., Khalid, I., Hussain, L., Imam, M.T., Shahid, I., 2023. Topical delivery of terbinafine HCL using nanogels: a new approach to superficial fungal infection treatment. Gels 9 (11), 841. https://doi.org/10.3390/gels9110841.

Hemmingsen, L.M., Škalko-Basnet, N., Jøraholmen, M.W., 2021. The expanded role of chitosan in localized antimicrobial therapy. Mar. Drugs 19 (12), 697. https://doi.org/10.3390/md19120697.

Heredia, N.S., Vizuete, K., Flores-Calero, M., Pazmiño, V.K., Pilaquinga, F., Kumar, B., Debut, A., 2022. Comparative statistical analysis of the release kinetics models for nanoprecipitated drug delivery systems based on poly(lactic-co-glycolic acid). PLoS One 17 (3), e0264825. https://doi.org/10.1371/journal.pone.0264825.

Hintze, V., Schnabelrauch, M., Rother, S., 2022. Chemical modification of hyaluronan and their biomedical applications. Front. Chem. 10, 830671. https://doi.org/10.3389/fchem.2022.830671.

Idrees, H., Zaidi, S.Z.J., Sabir, A., Khan, R.U., Zhang, X., Hassan, S., 2020. A review of biodegradable natural polymer-based nanoparticles for drug delivery applications. Nanomaterials 10 (10), 1970. https://doi.org/10.3390/nano10101970.

Jain, N., Verma, A., Jain, N., 2020. Formulation and investigation of pilocarpine hydrochloride niosomal gels for the treatment of glaucoma: Intraocular pressure measurement in white albino rabbits. Drug Deliv. 27 (1), 888–899. https://doi.org/10.1080/10717544.2020.1775726.

Jeon, S., Yoo, C.Y., Park, S.N., 2015. Improved stability and skin permeability of sodium hyaluronate-chitosan multilayered liposomes by Layer-by-Layer electrostatic deposition for quercetin delivery. Colloids Surf. B Biointerfaces 129, 7–14. https://doi.org/10.1016/j.colsurfb.2015.03.018.

Junyaprasert, V.B., Singhsa, P., Suksiriworapong, J., Chantasart, D., 2012. Physicochemical properties and skin permeation of Span 60/Tween 60 niosomes of ellagic acid. Int. J. Pharm. 423 (2), 303–311. https://doi.org/10.1016/j.ijpharm.2011.11.032.

Karuppaiah, A., Siram, K., Hariharan, S., Santhanam, R., Bharath, S., 2020. Development and evaluation of a pH triggered in situ ocular gel of brimonidine tartrate. J. Res. Pharm. 24 (3), 416–424. https://doi.org/10.35333/jrp.2020.164.

Khalid, W., Shah, K.U., Saeed, M.D., Nawaz, A., Rehman, F.U., Shoaib, M., Rehman, M. U., Alasmari, A.F., Alharbi, M., Alasmari, F., 2023. 5-Fluorouracil-loaded hyaluronic acid-coated niosomal vesicles: fabrication and ex vivo evaluation for skin drug delivery. ACS Omega 8 (48), 45405–45413. https://doi.org/10.1021/acsomega.3c04457.

Khallaf, R.A., Aboud, H.M., Sayed, O.M., 2020. Surface modified niosomes of olanzapine for brain targeting via nasal route; preparation, optimization, and in vivo evaluation. J. Liposome Res. 30 (2), 163–173. https://doi.org/10.1080/08982104.2019.1610435.

Khan, D.H., Bashir, S., Khan, M.I., Figueiredo, P., Santos, H.A., Peltonen, L., 2020. Formulation optimization and in vitro characterization of rifampicin and ceftriaxone dual drug loaded niosomes with high energy probe sonication technique. J. Drug Delivery Sci. Technol. 58, 101763. https://doi.org/10.1016/j.jddst.2020.101763.

Khatoon, M., Shah, K.U., Din, F.U., Shah, S.U., Rehman, A.U., Dilawar, N., Khan, A.N., 2017. Proniosomes derived niosomes: Recent advancements in drug delivery and targeting. Drug Deliv. 24 (2), 56–69. https://doi.org/10.1080/10717544.2017.1384520.

Kumar, M., Tiwari, A., Asdaq, S.M.B., Nair, A.B., Bhatt, S., Shinu, P., Al Mouslem, A.K., Jacob, S., Alamri, A.S., Alsanie, W.F., Alhomrani, M., Tiwari, V., Devi, S., Pathania, A., Sreeharsha, N., 2022. Itraconazole loaded nano-structured lipid carrier for topical ocular delivery: optimization and evaluation. Saudi J. Bio. Sci. 29 (1), 1–10. https://doi.org/10.1016/j.sjbs.2021.11.006.

Landucci, E., Mazzantini, C., Calvani, M., Pellegrini-Giampietro, D.E., Bergonzi, M.C., 2023. Evaluation of conventional and hyaluronic acid-coated thymoquinone liposomes in an in vitro model of dry eye. Pharmaceutics 15 (2), 578. https://doi.org/10.3390/pharmaceutics15020578.

Mehrandish, S., Mirzaeei, S., 2020. A review on ocular novel drug delivery systems of antifungal drugs: functional evaluation and comparison of conventional and novel dosage forms. Adv. Pharm. Bull. 11 (1), 28–38. https://doi.org/10.34172/apb.2021.003.

Miatmoko, A., Safitri, S., Aquila, F., Cahyani, D., Hariawan, B., Hendrianto, E., Hendradi, E., Sari, R., 2021. Characterization and distribution of niosomes containing ursolic acid coated with chitosan layer. Res. Pharm. Sci. 16 (6), 660. https://doi.org/10.4103/1735-5362.327512.

Nemr, A.A., El-Mahrouk, G.M., Badie, H.A., 2022. Hyaluronic acid-enriched bilosomes: An approach to enhance ocular delivery of agomelatine via D-optimal design: formulation, in vitro characterization, and in vivo pharmacodynamic evaluation in rabbits. Drug Deliv. 29 (1), 2343–2356. https://doi.org/10.1080/10717544.2022.2100513.

Ning, M., Guo, Y., Pan, H., Chen, X., Gu, Z., 2005. Preparation, in vitro and in vivo evaluation of liposomal/niosomal gel delivery systems for clotrimazole. Drug Dev. Ind. Pharm. 31 (4–5), 375–383. https://doi.org/10.1081/DDC-54315.

Padmasri, B., Nagaraju, R., 2021. Formulation development and evaluation of itraconazole ocular in-situ gel for enhancement of ocular bioavailability: in-vitro antifungal activities assessment. Int. J. Pharm. Sci. Rev. Res. 66 (1), 136–141. https://doi.org/10.47583/ijpsrr.2021.v66i01.022.

Pandit, J., Sultana, Y., Aqil, M., 2021. Chitosan coated nanoparticles for efficient delivery of bevacizumab in the posterior ocular tissues via subconjunctival administration. Carbohydr. Polym. 267, 118217. https://doi.org/10.1016/j.carbpol.2021.118217.

Permana, A.D., Utami, R.N., Layadi, P., Himawan, A., Juniarti, N., Anjani, Q.K., Utomo, E., Mardikasari, S.A., Arjuna, A., Donnelly, R.F., 2021. Thermosensitive and mucoadhesive in situ ocular gel for effective local delivery and antifungal activity of itraconazole nanocrystal in the treatment of fungal keratitis. Int. J. Pharm. 602, 120623. https://doi.org/10.1016/j.ijpharm.2021.120623.

Pourseif, T., Ghafelehbashi, R., Abdihaji, M., Radan, N., Kaffash, E., Heydari, M., Naseroleslami, M., Mousavi-Niri, N., Akbarzadeh, I., Ren, Q., 2023. Chitosan -based nanoniosome for potential wound healing applications: Synergy of controlled drug release and antibacterial activity. Int. J. Biol. Macromol. 230, 123185. https://doi.org/10.1016/j.ijbiomac.2023.123185.

Pramanik, A., Sahoo, R.N., Nanda, A., Pattnaik, K.P., Mallick, S., 2020. Swelling Kinetics and Corneal Hydration Level of Kaolinin-HPMC Hydrogel Film. Indian J. Pharm. Sci. 82 (2). https://doi.org/10.36468/pharmaceutical-sciences.651.

Puluhulawa, L.E., Joni, I.M., Elamin, K.M., Mohammed, A.F.A., Muchtaridi, M., Wathoni, N., 2022. Chitosan–hyaluronic acid nanoparticles for active targeting in cancer therapy. Polymers 14 (16), 3410. https://doi.org/10.3390/polym14163410.

Roque, L., Fernández, M., Benito, J.M., Escudero, I., 2020. Stability and characterization studies of Span 80 niosomes modified with CTAB in the presence of NaCl. Colloids Surf. A Physicochem. Eng. Asp. 601, 124999. https://doi.org/10.1016/j.colsurfa.2020.124999.

Sebaaly, C., Trifan, A., Sieniawska, E., Greige-Gerges, H., 2021. Chitosan-coating effect on the characteristics of liposomes: a focus on bioactive compounds and essential oils: a review. Processes 9 (3), 445. https://doi.org/10.3390/pr9030445.

Sheshala, R., Ming, N.J., Kok, Y.Y., Raj Singh, T.R., Dua, K., 2019. Formulation and characterization of ph induced in situ gels containing sulfacetamide sodium for ocular drug delivery: a combination of Carbopol®/ HPMC Polymer. Ind. J. Pharm. Edu. Res. 53 (4), 654–662. https://doi.org/10.5530/ijper.53.4.127.

Sionkowska, A., Gadomska, M., Musiał, K., Piątek, J., 2020. Hyaluronic acid as a component of natural polymer blends for biomedical applications: a review. Molecules 25 (18), 4035. https://doi.org/10.3390/molecules25184035.

Supachawaroj, N., Damrongrungruang, T., Limsitthichaikoon, S., 2021. Formulation development and evaluation of lidocaine hydrochloride loaded in chitosan-pectin-hyaluronic acid polyelectrolyte complex for dry socket treatment. Saudi Pharm. J. 29 (9), 1070–1081. https://doi.org/10.1016/j.jsps.2021.07.007.

Taymouri, S., Varshosaz, J., 2016. Effect of different types of surfactants on the physical properties and stability of carvedilol nano-niosomes. Adv. Biomed. Res. 5 (1), 48. https://doi.org/10.4103/2277-9175.178781.

Tulbah, A.S., Elkomy, M.H., Zaki, R.M., Eid, H.M., Eissa, E.M., Ali, A.A., Yassin, H.A., Aldosari, B.N., Naguib, I.A., Hassan, A.H., 2023. Novel nasal niosomes loaded with lacosamide and coated with chitosan: A possible pathway to target the brain to control partial-onset seizures. Int. J. Pharm.: X 6, 100206. https://doi.org/10.1016/j.ijpx.2023.100206.

Tyagi, R., Waheed, A., Kumar, N., Mujeeb, M., Naved, T., Rashid Khan, M., Alhosaini, K., Alqarni, Y.A., Rahat, R., Alam, P., Madan, S., 2023. In-vitro and ex-vivo antidiabetic, and antioxidant activities of Box-Behnken design optimized Solanum xanthocarpum

extract loaded niosomes. Saudi Pharm. J. 31 (10), 101785. https://doi.org/10.1016/j.jsps.2023.101785.
Valachová, K., Šoltés, L., 2021. Versatile Use of Chitosan and Hyaluronan in Medicine. Molecules 26 (4), 1195. https://doi.org/10.3390/molecules26041195.
Verma, A., Tiwari, A., Saraf, S., Panda, P.K., Jain, A., Jain, S.K., 2021. Emerging potential of niosomes in ocular delivery. Expert Opin. Drug Deliv. 18 (1), 55–71. https://doi.org/10.1080/17425247.2020.1822322.
Yoo, C.Y., Seong, J.S., Park, S.N., 2016. Preparation of novel capsosome with liposomal core by layer-by-Layer self-assembly of sodium hyaluronate and chitosan. Colloids Surf. B Biointerfaces 144, 99–107. https://doi.org/10.1016/j.colsurfb.2016.04.010.
Zeng, W., Li, Q., Wan, T., Liu, C., Pan, W., Wu, Z., Zhang, G., Pan, J., Qin, M., Lin, Y., Wu, C., Xu, Y., 2016. Hyaluronic acid-coated niosomes facilitate tacrolimus ocular delivery: Mucoadhesion, precorneal retention, aqueous humor pharmacokinetics, and transcorneal permeability. Colloids Surf. B Biointerfaces 141, 28–35. https://doi.org/10.1016/j.colsurfb.2016.01.014.
Zhang, X., Wei, D., Xu, Y., Zhu, Q., 2021. Hyaluronic acid in ocular drug delivery. Carbohydr. Polym. 264, 118006. https://doi.org/10.1016/j.carbpol.2021.118006.
Zubairu, Y., Negi, L.M., Iqbal, Z., Talegaonkar, S., 2015. Design and development of novel bioadhesive niosomal formulation for the transcorneal delivery of anti-infective agent: In-vitro and ex-vivo investigations. Asian J. Pharm. Sci. 10 (4), 322–330. https://doi.org/10.1016/j.ajps.2015.02.001.